

**Metal organic frameworks for photo-catalytic water splitting**

Journal:	<i>Energy & Environmental Science</i>
Manuscript ID:	EE-PER-01-2015-000161.R2
Article Type:	Perspective
Date Submitted by the Author:	22-May-2015
Complete List of Authors:	Meyer, Kim; ETH Zurich, Chemical and Bioengineering Ranocchiari, Marco; Paul Scherrer Institut, SYN; van Bokhoven, Jeroen; Paul Scherrer Institut, SYN; ETH Zurich, Chemical and Bioengineering

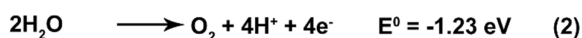
Metal organic frameworks for photo-catalytic water splitting

K. Meyer,^a M. Ranocchiari^b and J. A. van Bokhoven^{a, b}

Metal organic frameworks (MOFs) have recently debuted as participants and solid supports in catalytic water splitting. Their porosity and structural versatility offer a tantalising consolidation of the components needed for solar light harvesting and water splitting. Herein, we describe a selection of relevant contemporary investigations that employ electrocatalysis, chemically introduced redox partners, and photo-catalysts to generate dioxygen and dihydrogen from water. The role of semiconducting MOFs in these systems is addressed, in tandem with band gap control by linker functionalisation and doping. Considered holistically, MOFs offer an impressive physical, spatial and chemical versatility with which to support and sustain water splitting reactions. Major challenges toward practical implementation do remain, but opportunities for development are evidently numerous.

Introduction

Fossil fuel reserves are dwindling and their unrestricted use has led to incontrovertible changes in the Earth's surface temperature and climate.¹ Dihydrogen is a possible intermediate energy carrier. However, for economic reasons industrial scale dihydrogen production continues to depend on fossil fuels.² At present steam reforming of natural gas and oil, as well as coal gasification, contribute 96% of the world's dihydrogen supply.³ Even electrocatalytic water splitting relies on vast quantities of fossil fuel derived energy to perform the thermodynamically uphill process with a ΔG^0 of 113 kcal/mol.⁴ The water oxidation half reaction is more demanding than the reduction process (Scheme 1), with a minimum potential of 1.23 V per electron transfer.



Scheme 1 Proton reduction (1) and water oxidation (2) half reactions (NHE, 25°C, pH 0).

Numerous homogeneous and heterogeneous water oxidation (WOCs) and reduction catalysts (WRCs) have been developed with the intention of accessing low energy pathways to dioxygen and dihydrogen, and some of these are able to harness the energy from the UV-visible portion of the solar spectrum.⁵⁻⁹ The prodigious exergy of incidental sunlight striking the Earth's surface (86 Petawatts) represents humanity's most bountiful energy resource, and methods by which it might be harnessed are eagerly sought.¹⁰ Natural systems have evolved to capitalise on solar energy, but as yet very few man-made assemblies are able to match the prowess of dioxygen evolving photosystem II (100-400 s⁻¹) and the impressive dihydrogen evolution of [FeFe] hydrogenase (TON 10⁴ s⁻¹).^{11, 12} These remarkable biocatalysts are truly challenging to mimic because their activity is under-pinned by a complex array of inter-connected components that spatially and chemically influence the catalytic site, while preventing deactivation caused by charge build-up and recombination. In the case of photosynthesis, PSI and PSII photo-catalysts are connected by an elaborate electron transport chain, and protons are shuttled to biochemical cycles that lead to manufacture of sugars.¹³ Dubbed the Z-scheme, this remarkable two photon-dual band gap process is able to establish an electrochemical gradient across a non-conducting membrane.¹⁴

Nature's photosynthetic Z-scheme offers a useful framework upon which to model artificial photo-catalysed water splitting.¹⁵ In Fig. 1, Z-scheme water splitting is depicted as two photon excitation events occurring in dual light

absorbers with band gaps configured for water oxidation and reduction. Half-reactions are driven by photo-excited electrons and holes promoted to the conduction and valence bands of each material, respectively. An acceptor-donor relay translates redox changes between the two photo-absorbers. Sacrificial acceptors or donors may also be employed to aid in the study of half-reactions through regeneration of catalysts or scavenging of destructive by-products. Depending on the unique electronic requirements of an *anthropogenic Z-scheme*-like water splitting system or an isolated water oxidation or reduction half-reaction intervention of light sensitisers, co-catalysts, redox mediators, sacrificial donors or acceptors may be required in addition to the catalyst itself. *Photochemical* or *chemical* water splitting half-reactions sometimes employ sensitisers ($[\text{Ru}(\text{bpy})_3]^{2+}$ or its substituted derivatives, porphyrins or organic dyes),¹⁶ electron donors (ethanolamines, triethylamine, alcohols, EDTA, L-ascorbic acid, Γ^- , SO_3^{2-} , S^{2-} , Fe^{2+} or Ce^{3+}), or electron acceptors (Ce^{4+} , IO_4^- , $\text{S}_2\text{O}_8^{2-}$, $[\text{Ru}(\text{bpy})_3]^{3+}$, IrCl_6^{2-} , $[\text{Fe}(\text{phen})_3]^{3+}$, K-oxone or OCl^-).^{6,9}

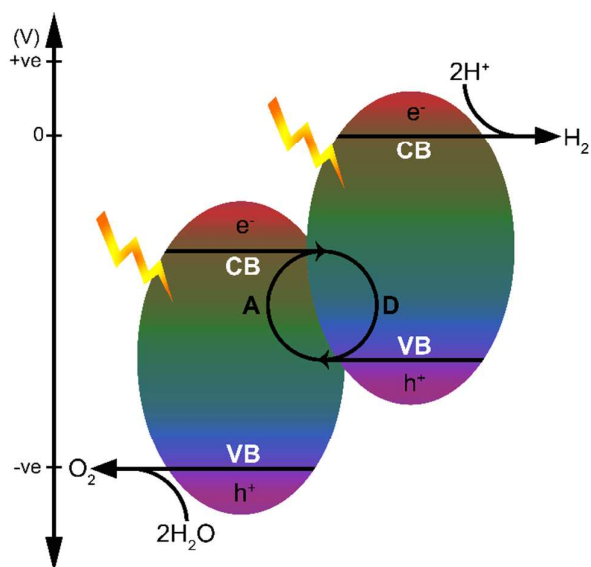


Fig. 1 A conceptual two-photon Z-scheme for photo-catalysed water oxidation and reduction half-reactions mediated by holes (h^+) populating the valence band (VB) and electrons (e^-) occupying the conduction band (CB), respectively. In the reduction half reaction a donor (D)-acceptor (A) redox mediator is oxidised by holes while photo-formed electrons go on to reduce H^+ into dihydrogen. Water oxidation occurs via a photo-formed hole and reduction of the redox mediator.

New echelons of solar-to-electric power (η) and solar-to-hydrogen conversion efficiencies (STH) have been reached by implementing affordable oxide-based semiconductors inside man-made photoelectrochemical (PEC) water splitting devices. Tandem cells are favoured because, up to a point, they allow maximisation of solar absorption via coupling of complementary photosystems.¹⁷ Commonly employed operation modes include; single band gap-two photon (S2), dual band gap-two photon (D2 i.e. the Z-scheme), dual band gap-four photon (D4), and triple band gap-six photon (T6) systems, comprising semiconductor layers interposed by junctions.¹⁸ Recent research endeavours have focused on the abundant semiconductor materials Cu_2O , $\alpha\text{-Fe}_2\text{O}_3$, BiVO_4 , WO_3 , crystalline (c-Si) and amorphous silicon (a-Si), and TiO_2 , which possess band gaps that may be tailored to participate in visible light absorption and water splitting.¹⁹ Researchers are faced with a perplexing dichotomy; S2 photocathodes generally have poor stability in water, whereas water stable photoanodes often possess overly large band gaps. Consequently, considerable effort is devoted to tackling the shortcomings of these semiconductors when

they are used in water cleavage devices, by; tandem coupling of band gaps, inclusion of solar cells, incorporation of catalysts or dopants, use of passivating layers, astutely constructed PEC cells or novel nano-scale structures. To give readers a flavour for the latest advancements in this vast and multi-disciplinary field, we provide a glancing perspective of the leading technologies below.

Among the most successful water splitting devices, Grätzel *et al.* have attained a 12.3% STH efficiency with an over-all current density of 10.0 mA cm^{-2} using tandem solar cells coupled with a bifunctional catalyst of layered NiFe double hydroxides grown on nickel foam.²⁰ Highly efficient $\text{CH}_3\text{NH}_3\text{PbI}_3$ perovskite solar cells with a 17.3% η account for much of the initial efficiency of this integrated system, but become its Achilles heel over time.²¹ In another approach, Grätzel *et al.* constructed a tandem dye-sensitised solar cell and mesoporous WO_3 photoanode device to obtain a 3.1% STH efficiency with a 2.52 mA cm^{-2} current density.²² The D4 device capitalised on the efficiency of a Y123 dye as a redox mediator between a cobalt-based photosensitiser and the WO_3 semiconductor catalyst.²³ Other groups have tackled the solar capture problem using tandem solar cells encompassing visible and infrared regions of the light spectrum. Tuner *et al.* obtained a 12.4% STH efficiency using a T6 PEC device comprising GaInP_2 (1.83 eV/ 678 nm band gap) and GaAs (1.42 eV/ 873 nm band gap) junctions, and a platinum electrode.²⁴ But at the expense of high production and material costs, and a limited lifetime. Current prototypes of the “artificial leaf”^{25, 26} achieve a 10% STH efficiency and a current density of 7.8 mA cm^{-2} using a c-Si photovoltaic device connected to a NiB_1 -anode/ NiMoZn -cathode electrochemical cell.²⁷ Here, the severe cost and stability considerations associated with silicon semiconductors may yet be mitigated using amorphous TiO_2 coatings to protect against photo-corrosion.²⁸ A PEC device with unparalleled stability under field conditions was built from triple-junction a-Si photoelectrodes, and NiFe_yO_x (WOC) and CoMo alloy (WRC) thin films, obtaining an STH efficiency of 7.8% over 7,200 hours. In this system embedding of the vulnerable silicon photocathode between thin films of the catalysts translated to remarkable stability in an aqueous 1M KOH electrolyte, while a bespoke Plexiglas™ reactor allowed separation of dioxygen and dihydrogen into two separate streams.²⁹

Nano-scale fabrication has played an important physical role in addressing the inadequacies of semiconductor materials in PEC devices. In particular, nanorods or wires offer a large available surface area for addition of dopants such as light absorbers, catalysts, charge carriers or passivators; while also providing a framework for construction of buried junctions and dimensionally optimised semiconductor arrays calculated to maximise PEC efficiency. In a direct allegory of the Z-scheme, Yang *et al.* devised “nanotree” heterostructures with silicon trunks and rutile TiO_2 branches. Although η efficiency was poor, a compelling facet of this prototype was that the density of TiO_2 photoanodes – the limiting photoelectrode for water splitting in this device – was modifiable.³⁰ In another dual band gap device Lewis *et al.* demonstrated the efficacy of buried homojunction np^+ -Si microwires layered with ITO and WO_3 for optimising charge collection and light absorption path lengths.³¹ Much mileage has been gained in using nanorod architectures to counter the poor carrier collection distances in Fe_2O_3 , a material with an otherwise lucrative $\sim 2.1 \text{ eV}$ band gap encompassing 40% of the solar spectrum. On this front Lee *et al.* have obtained a record current density of 4.32 mA cm^{-2} from Fe_2O_3 “worm-like” photoanodes bulk-doped with platinum and surface-doped with Co-Pi cocatalyst.³² Similarly, van de Krol *et al.* made significant improvements to the charge separation capabilities of a BiVO_4 semiconductor by introducing a 10-step 1-0% tungsten dopant gradient between the thin film interface and back contact, thereby distributing an n+-n homojunction across the bulk of the film. Once assembled into a triple junction PEC device comprising an a-Si photovoltaic cell and W: BiVO_4 photoanode deposited with Co-Pi, a current density of 4 mA cm^{-2} and STH efficiency of 4.9% was obtained.³³

An overarching principle becomes evident when we step back and consider the substantial creativity and ingenuity employed in construction of state-of-the-art PEC water splitting devices. In the absence of a single “fit-for-purpose”

semiconductor it appears that *adaptability* is an essential requirement of any material vying for credibility in the race towards efficient and inexpensive photo-activated water splitting catalysts. Metal organic frameworks (MOFs) occupy an intriguing and versatile position on the spectrum of feasible contenders. Not only do their physical, chemical and electronic properties marry the recyclability benefits of heterogeneous catalysis to the defined ligand environments of homogeneous catalysis, but certain MOFs also borrow electronic attributes from semiconductor materials.

Fundamental aspects of MOFs

MOFs utilise the driving impetus of coordination chemistry to assemble multidentate organic or organometallic linkers around metal secondary building units (SBUs), forming 2D and 3D coordination polymers with well-defined topologies (Fig. 2a). A staggering range of MOF compositions and topologies have been reported since the class was first coined by Yaghi in 1995.³⁴ These hybrid inorganic-organic crystalline materials are best known for their large porosity and internal surface area spanning micro- and mesoporous ranges, which renders them excellent candidates for gas adsorption and separation – dihydrogen among them.³⁵ MOFs are capable of remarkable physical contortions in response to adsorption and desorption of guest molecules, thermal and photon irradiation, as well as mechanical force. Frameworks are known to demonstrate swelling, “breathing,” linker rotation and rearrangement, subnetwork displacement, and phase changes induced by deformations at SBUs.³⁶ Within the large MOF family examples may be found of dynamic magnetism,³⁷ electrical conductivity,³⁸ luminescence³⁹ and tuneable light absorption.^{40, 41} Structuring of MOFs into complex meso- or macroscopic architectures has been achieved in recent years thanks to templating, confinement, liquid-liquid or liquid-solid interfacial reactions and top-down processing techniques. The scope of 0, 1, 2 or 3D superstructures that are accessible provide useful conformational control over MOFs that may translate well to applications where thin films, hollow spheres, or membranes are required.⁴² The isoreticularity of MOFs may be exploited to tune their properties - a characteristic which allows chemical and steric modification at the organic linker with preservation of framework topology. Thanks to the strength of their coordinate bonds, the frameworks of many of these coordination polymers demonstrate high thermal and chemical stability, and consequently chemical transformations may be carried out on intrinsic functional groups or single-sites. In this regard post-synthetic modification techniques, where the functional groups inside a parent MOF are transformed into a specific target group, have played a crucial role in achieving diverse functionalisation, responses and reactivities.⁴³

The customisable nature of MOF synthesis allows rational design of frameworks so that they contain specific features, such as a large surface area and porosity, as well as stability in elected media.⁴⁴ But beyond physical attributes, frameworks may also be designed with an electronic goal in mind. Recent prospective publications highlight the practical aspects of using MOFs in electronic devices – a research field coined “MOFtronics.”^{45, 46} Some MOFs present characteristics that are favourable for charge capture and transport, including extended networks, photo-receptive inorganic nodes and linkers, electronically tuneable π -conjugated organic linkers and adjustable band gaps. As we will explain, a small number of these materials possess semiconducting properties and may use the energy of light to drive catalysis due to advantageously aligned valence and conduction bands between the light antennae and catalyst.

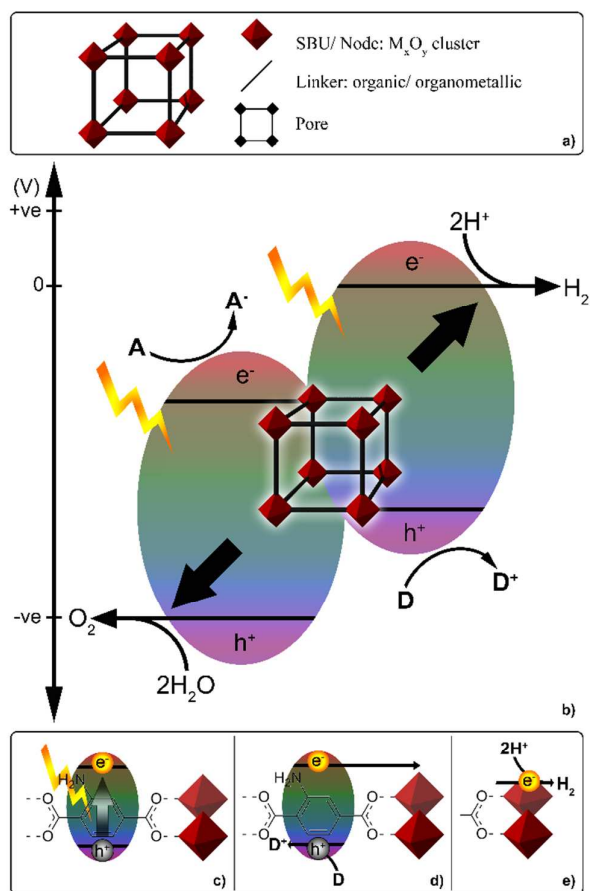


Fig. 2 (a) The inorganic node (SBU) and organic linker are the basic components of a MOF. These may be varied and modified post-synthetically to obtain structures with different pore sizes, connectivity and chemical functionality, thus rendering them ideal candidates for engineered water splitting systems; (b) conceptual schematic for photo-catalysed water oxidation or reduction using a MOF in the presence of an acceptor or donor, respectively. On the right photo-generated electrons reduce H⁺ while concurrently produced holes oxidise introduced donors. On the left photo-generated holes oxidise water while concurrently produced electrons reduce introduced acceptors; (c) light harvesting accomplished by an organic linker; (d) generation of a charge separated state and quenching of h⁺ by a donor; (e) electron transfer to the metal oxide node and subsequent proton reduction.

In Fig. 2b we present a conceptual photo-activated MOF with catalytic water oxidation or reduction capabilities. An assembly of this type uses the energy of sunlight to generate long-lived charge-separated states that allow transfer of holes to WOCs embedded in or grafted onto the framework, while the complimentary electron is absorbed. Likewise, such a system could enable free transport of photo-generated electrons to sites for water reduction, while the complimentary hole oxidises a donor. For the purposes of clarity, a representative photo-catalysed water reduction process is depicted in panels Fig. 2c, 2d and 2e; demonstrating photo-excitation, formation of a charge separated state, and electron transfer respectively. While a WRC must transfer only two electrons to a commensurate quantity of H⁺ to generate dihydrogen, a WOC must relay four available holes to water via a series of steps with a combined free energy of 4.92 eV (4 × 1.23 eV).⁴⁷ Production of dihydrogen from water is thus dependent on the hefty electrochemical requirements of water oxidation.

MOFs are beginning to distinguish themselves as viable participants and solid supports in catalytic processes.^{48, 49} They have made a debut in photo-catalysed processes where certain chemical transformations, such as CO₂

reduction, dihydrogen evolution and water splitting are concerned.⁵⁰ It is their direct electronic and photonic responsivity that differentiates MOFs from comparable crystalline porous materials such as zeolites,⁵¹ which are among the select materials utilised as solid supports in photo-catalytic water splitting.⁵² By comparison, aluminosilicates are band gap insulators that are transparent to UV-visible wavelengths. They are typically only used in electronics or photonics applications in the capacity of hosts for conductive or photo-active guests, respectively,^{53, 54} and while being very robust, the rigid tetrahedra that make up their skeletons severely hinder structural tailoring.

In this review we highlight a number of key considerations and developments in the MOF water splitting field, including stability under aqueous conditions, new water oxidation and reduction catalysts, and the exposition of these materials in electrolytic, chemically promoted and photo-catalytic settings. Classical MOF characteristics offer many benefits to water splitting processes, such as; large surface areas allowing high density of catalytic sites in precisely delineated spatial and chemical environments, porosity for unrestricted transport of participatory chemical agents, encapsulated protection for sensitive catalysts and their intermediates, thermal tolerance, and facile fabrication. In addition, we feel that MOFs offer a compelling modularity. In a 2013 news release by Sandia National Laboratories, MOFs were likened to “tinkertoys,” the “ultimate, small-scale unit” for construction of electronic devices.⁵⁵ It is this capacity which sets MOFs apart from other materials and devices, because it allows researchers to easily apply tuning pegs to a multitude of baseline properties (light absorption and electrical conductivity among them). Starting from a vast library of already discovered coordination polymers, MOFs have the potential to impart mutable physical, chemical and electrical properties to photo-catalysed water splitting. It is our hope to inspire further research by showcasing the latest strategies and innovations currently employed in the field.

MOF stability under water splitting conditions. The robustness of a framework toward water is fundamentally dependent on the strength of its metal_{node}-O_{linker} or metal_{node}-N_{linker} bonds, a characteristic which is governed by the pK_a of the linker and the Lewis acidity of the coordinated metal. For a detailed account of MOF stability under specifically aqueous conditions we direct readers to a number of useful reviews.⁵⁶⁻⁵⁸ To participate in water *splitting* a MOF should demonstrate stability under aqueous conditions and may also need to tolerate other factors. Solution pH can be influential where strongly acidic conditions (e.g. water oxidation using sacrificial oxidant Ce⁴⁺)⁵⁹ or basic conditions (e.g. water reduction in the presence of sacrificial donors such as triethylamine) are called for. Additional sensitisers, sacrificial acceptors and donors necessary to support water oxidation or reduction may also have deleterious effects on the integrity of a framework. Given the vast number of MOF morphologies and metal-linker combinations accessible,⁶⁰ as well as the array of chemical conditions utilised to perform water splitting, it is evidently necessary to evaluate the stability requirements of each system on a case by case basis.

Notable frameworks that are likely to support the rigours of water splitting include; UiO-66 (Zr) and UiO-67 (Zr),^{61, 62} MIL-100 (Cr),⁶³ MIL-101 (Al and Cr),^{64, 65} MIL-53 (Al and Cr),^{66, 67} MIL-125 (Ti),⁶⁸ ZIF-8 (Zn),⁶⁹ several PCN (Zr-porphyrins)^{70, 71} and SIM-1 (Zn).⁷² Within these families of diverse MOFs a range of specific aptitudes are found. ZIF-8 (Zn) and MIL-100 (Cr) are stable in water for months under ambient conditions, the UiO-66 (Zr) framework survives boiling in water for hours,⁷³ MIL-101 topologies are tolerant of strongly acidic media, and PCN-222 retains crystallinity between a pH of 1 and 11. While a number of different types of MOFs do participate in water oxidation and reduction catalysis, UiO-66, UiO-67, MIL-101 and MIL-125 materials appear most frequently.

MOF supported electrocatalytically driven water splitting. During water electrolysis an applied potential is used to split molecules into H^+ and OH^- . Simplistically speaking, an electrocatalytic system eliminates many of the complexities of the Z-scheme, because the cathode (reducing electrode) and the anode (oxidising electrode) mediate direct reduction of H^+ into dihydrogen and oxidation of OH^- into dioxygen respectively, when a sufficient overpotential is applied. As such, electrocatalytic devices comprising a WOC supported on an anode, or a WRC mounted on a cathode, provide a relatively straightforward means to harness the catalytic current of a suitable heterogeneous material. A comprehensive account of key developments in electrocatalytic and photo-electrocatalytic water splitting are reported in a number of descriptive reviews.^{16, 74-77}

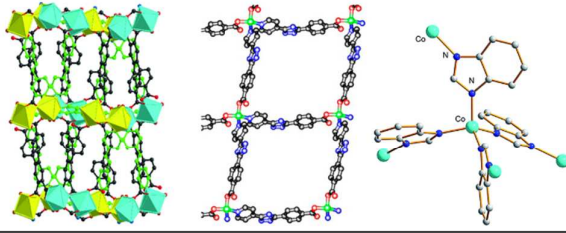
Only a handful of MOFs have been reported that are capable of performing electrocatalytically driven water oxidation and reduction. In Table 1 we have presented several of these studies, which possess few structural similarities aside from the fact that they all contain cobalt. Other more exotic systems, such as manganese containing POMs and 3d-4f MOFs, have also been reported.^{78, 79} In some of these studies the catalytic activity was of a dualistic nature – that is the MOF was able to generate both dioxygen and dihydrogen upon application of a current. This fact alone advocates use of MOFs in electrocatalytic water splitting, although the exact nature of the active sites involved still requires careful examination.

Gong *et al.* describe electrocatalysed dual water splitting for 2D and 3D Co(II) coordination polymers based on mixed linkers.⁸⁰ The two prepared systems, which are composed of 4,5-di(4'-carboxylphenyl)phthalic acid and a bidentate nitrogen ligand (4,4'-bipy or (*E*)-1,2-di(pyridine-4-yl)diazene), reveal both reductive and oxidative currents when mounted in Nafion on a glassy carbon electrode (GCE). The azene adduct is the more active of the two systems, operating at turnover numbers (TONs) of 7.88 mol of dioxygen and 1.67 mol of dihydrogen per mole of complex (Entry 1, Table 1; H_3PO_4 / KOH buffer pH 6.8, SCE and platinum electrodes). Contributions to catalysis by the organic constituents were very low and easily distinguished by their unique features in a cyclic voltammogram, thereby ruling out decomposition products as the catalytically active agents. The implications of this study are that the bulk of the dual catalytic functionality arises from the framework itself – be it via the targeted intervention of specific Co(II) centres (cobalt assumes two unique coordination environments within each individual framework) or metal nuclei acting in tandem.

Likewise, isostructural cobalt and copper MOFs constructed from a rigid 4-(5-(pyridine-4-yl)-4H-1,2,4-triazol-3-yl)benzoic acid linker catalysed water oxidation and reduction once adsorbed to Nafion and mounted on a GCE.⁸¹ These 2D frameworks were characterised by four-coordinate tetrahedral cobalt nodes attached to the linker via its pyridine nitrogen and mono-carboxylate functional groups. While stable for electrocatalytic water *reduction*, the cobalt complex did not survive water *oxidation* and eventually dissolved. Despite this impediment the material achieved TONs of 1.92 mol for dihydrogen and 6.73 mol for dioxygen in two hours (Entry 2, Table 1; H_3PO_4 / KOH buffer pH 6.8, SCE and platinum electrodes). By comparison, the copper adduct of this MOF exhibited a third of the oxygen evolving activity due to a markedly more positive overpotential for the oxidation half reaction.

A purely imidazolite framework, Co-ZIF-9, demonstrated exclusive oxygen evolution from water when coated on a fluorine doped tin oxide (FTO) glass slide and subjected to a current (phosphate buffer pH 6.8, Ag/AgCl reference electrode).⁸² Constructed from tetrahedral Co(II) and four equivalents of benzimidazole linker, this catalyst generated 8 μ mol of dioxygen within three hours, with a turnover frequency (TOF) of $1.76 \times 10^{-3} \text{ s}^{-1}$ (Entry 3, Table 1). Strongly basic electrolytes reduced the overpotential for oxygen evolution, and may also have played a part in lowering the energy barrier toward formation of a crucial Co-OH intermediate. DFT calculations infer the importance of a dehydrogenation step, in which adsorbed water relinquishes a single hydrogen atom to the azolium CH component of a coordinated benzimidazolium ligand, thus forming a dihydrobenzimidazole.

Table 1 Selected characteristics of electrocatalytically active cobalt-containing MOFs for water oxidation and reduction (* 8 μmol , TOF = $\sim 1.76 \times 10^{-3} \text{ s}^{-1}$). Adapted in part with the permission of the © Royal Society of Chemistry 2014, © the American Chemical Society 2012 and 2013, and © John Wiley and Sons 2014.



Entry	1	2	3
TON O ₂ (mol/mole cat.)	7.88	6.73	*
TON H ₂ (mol/mole cat.)	1.67	1.92	–
Time (h)	2	2	3
Active site	Co	Co	Co
Ref.	80	81	82

Given that MOFs are experimentally capable of catalysing both water oxidation and reduction under electrolytic conditions, the question remains: how should dihydrogen and dioxygen be separated from one another in a fully-fledged water splitting MOF? Custom-made electrocatalytic cells, like that prepared by Selli *et al.*, may provide an answer in the form of photo-active electrodes segregated into oxidising and reducing hemispheres that vent into two independent headspaces separated by an exchange membrane.^{83, 84} While this strategy is not inconceivable – techniques for growth of MOFs onto electrode surfaces are in development⁸⁵ – it is restrictive because it requires that parallel engineering challenges be met before a credible device may be realised. Electron-coupled-proton buffers (ECPBs) offer a compelling method for dioxygen generation which is decoupled from simultaneous dihydrogen production. Cronin *et al.* used the ECPB $[\text{H}_3\text{O}]^+[\text{H}_2\text{PMo}_{12}\text{O}_{40}]^-$ to “store” the electrons and protons generated during water splitting.⁸⁶ Remarkably, the lifetime of the buffer spanned many months, allowing retrieval of the stored protons and electrons at a time long after the event of dioxygen production. Simple quinones, so prevalent in natural photosynthetic electron transfer pathways,⁸⁷ are also viable ECPBs in artificial water splitting systems. Moreover, sulfonated hydroquinone/benzoquinone ECPB is highly soluble in water,⁸⁸ and quinone molecules are small enough to allow transport through the constricted pores and channels of MOFs. However, there are non-trivial considerations associated with this strategy too. A quinone-type redox mediator for photo-catalysed water splitting should undergo reduction under a regime (pH, potential and radiant energy) that coincides with the water oxidation half-reaction, and remain both stable and soluble in water in its reduced form. A dual-compartment reactor, comprising independent electrolytic cells for water oxidation and ECPB reduction was recently described.⁸⁹

MOF supported water oxidation promoted by a sacrificial oxidant. As we will describe, WOCs may be heterogenised or encapsulated within a MOF so as to prevent deactivation processes such as recombination of excited states or intermolecular interactions. Conceptually, MOFs provide a porous structure pre-disposed to free transfer of reaction constituents of appropriate dimensions, such as electron acceptors and light sensitiser. For the purposes of simplicity, the water oxidation aspect of the water splitting Z-scheme may be simulated using a sacrificial chemical oxidant. A handful of MOF systems are capable of oxidising water in the presence of aggressive sacrificial oxidants, such as ceric ammonium nitrate (CAN). In particular, MIL-101(Cr) and UiO-67

type frameworks are sufficiently robust to undergo recycling where the catalytic site contained by the MOF is either homogeneous or heterogeneous in nature.

Homogeneous catalysts encapsulated inside MOFs represent the most active of known systems with respect to TOF versus catalyst concentration. A μ -oxo manganese terpyridine dimer (MnTD) modelled on the oxygen evolving complex in photosystem II undergoes 95% degradation upon onset of catalysis. Intermolecular interactions are evidently responsible for deactivation of this highly active complex into permanganate.⁹⁰ Das *et al.* sought to address the problem by assembling the complex inside porous materials, thereby preventing catalyst deactivation by isolating individual dimers in their own cages. Large caged materials, such as mesoporous silica FDU-12, hold more than one equivalent of the dimer, and consequently the catalyst is not protected from destructive interactions with other molecules and ceases to operate within seven hours.⁹¹ However, the internal cage dimensions of MIL-101 (Cr) are only sufficient to contain one dimer molecule per cage (Fig. 3), equating to a total catalyst loading of 10wt% relative to the MOF.⁹² Catalytic testing using the impregnated MOF in the presence of sacrificial oxidant K-oxone yielded a TOF of 0.02 (mol dioxygen/mole of caged manganese dimer) s^{-1} . While this value is half that of the un-encapsulated homogeneous complex, activity was sustained after 10 re-uses with no apparent decline in rate. Negligible catalytic conversion was observed from tests of the supernatant and a surface adsorbed version of the catalyst, thereby ruling out active leached and surface-only species. Use of an alternative sacrificial oxidant CAN (an oxygen-free electron acceptor with no possible culpability in dioxygen evolution) revealed a number of additional features. Namely, sustained catalysis in a pH 1 aqueous matrix over days, a TOF of 40 (mol dioxygen/mole of caged manganese dimer) h^{-1} with 4000 equivalents of CAN, and little sign of decomposition in the form of CO_2 . Eventual retardation of catalysis did occur, but is thought to be a result of pore clogging by cerium oxide particles rather than catalyst destruction.⁹¹

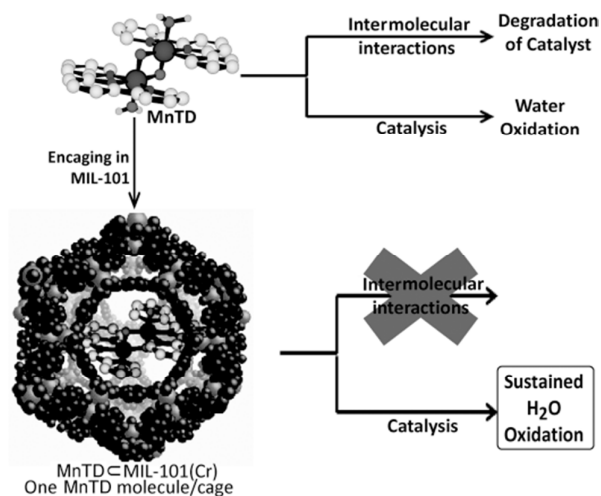


Fig. 3 Water oxidation catalysed by a μ -oxo manganese terpyridine dimer (MnTD) after encapsulation inside MIL-101 (Cr). Reproduced with permission from reference 49 © John Wiley and Sons.

Lin *et al.* prepared a series of integrated WOCs, where catalytically active sites were engineered upon an organic linker prior to MOF assembly. The IrCp*Cl motif was remarkably robust during assembly of the MOF in 100 °C DMF over 48 hours in the presence of the reactants trifluoroacetic acid and $ZrCl_4$. The resultant UiO-67 type frameworks possessed “expanded” (4,4'-([2,2'-bipyridine]-5,5'-diyl)dibenzoate or 4'-(5-(4-carboxylatophenyl)pyridin-2-yl)-[1,1'-biphenyl]-4-carboxylate)⁹³ and “contracted” ([2,2'-bipyridine]-5,5'-

dicarboxylate or 6-(4-carboxylatophenyl)nicotinate)⁹⁴ linkers coordinated to IrCp*Cl, see Fig. 4 (a) and (c) respectively. All MOFs were active in chemically promoted water oxidation using CAN, but the pore size of the contracted MOFs was apparently too small to permit permeation of CAN into the bulk material, thereby limiting catalysis to the particle surface and generating TOFs up to 16 times lower than that of the corresponding discrete linker complexes. By comparison, no diffusion limitation existed for the expanded systems and a TOF of 0.48 min⁻¹ was obtained over three consecutive re-uses. Evaluation of the supernatant after exposure to CAN revealed <1% leaching of iridium as well as the presence of acetic acid and formic acid. Evidently organic acids arise from oxidative modification of the coordinated Cp* on the way to the true catalytic intermediate, a proposed iridium chloro bis(aqua) adduct. This intermediate subsequently undergoes oxidation into the true WOC, an Ir(V)=O species (see Fig. 4 (b)). NMR spectroscopy indicated that after addition of 30 equivalents of CAN approximately 55% of the linkers had been modified, and of this approximately half consisted of the Ir(V)=O catalytically active adduct.

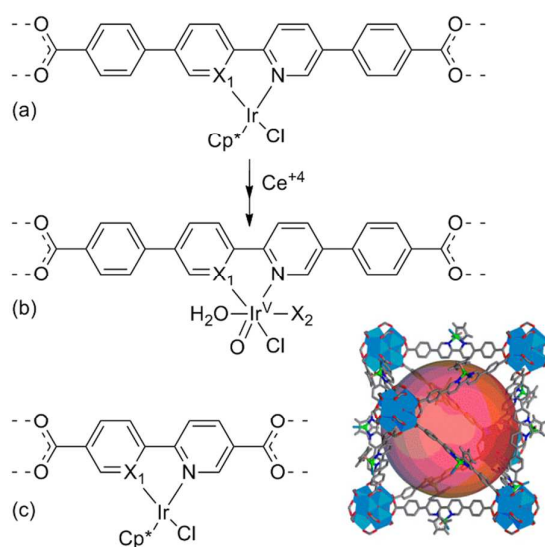


Fig. 4 UiO-67 (Zr) composed of (a) “expanded” and (c) “contracted” bipyridine or phenylpyridine linkers. Oxidative conversion of pre-catalyst (a) into an Ir(V)=O species (b) that is active in water oxidation ($X_1 = \text{N}/\text{C}$, $X_2 = \text{formate}/\text{acetate}$). Adapted with permission from reference 50 © American Chemical Society.

A recent study suggests that the high adsorptive capacity of MOFs for small molecules might be harnessed in challenging oxidation processes in combination with the innate redox properties of Fe-MOF-74. C-H activation of ethane to form ethanol was recently realised in activated hydroxyl-bound Fe(III) and mixed Fe/Mg 2,5-dioxido-1,4-benzenedicarboxylate MOFs (Fe-MOF-74).⁹⁵ In its inactivated form, the Fe(II) inorganic nodes of this system occupy square pyramidal coordination geometry and are easily accessible via wide hexagonal channels in the MOF architecture. The similarity of these iron sites to Fe-TAMLs, which are active in catalysed water oxidation, certainly bears some consideration.⁹⁶

Despite these highly promising developments in chemically promoted water oxidation catalysis supported by MOFs, an idealised system accomplishing photo-catalysed water oxidation remains elusive. At this stage it appears that the largest impediment to heterogeneously supported catalysis on UiO-67 lies in ensuring adequate diffusion of sacrificial oxidants to the mobilised catalytic sites. By contrast, MIL-101 (Cr) offers distinct advantages as a robust protective framework for chemically promoted homogeneous water oxidation where the catalyst is prone to self-

annihilation. We anticipate similar encapsulation experiments using $\text{Ru}(\text{bda})(\text{L})_2$ ($\text{bda} = 2,2'$ -bipyridine-6,6'-dicarboxylic acid, $\text{L} = 4$ -picoline or isoquinoline).⁹⁷ Li *et al.* have already found that encapsulation by mesoporous silica is catalytically advantageous for this highly active system due to enhanced co-operativity of the dimeric catalytic intermediate.⁹⁸

An intriguing, and yet unexplored avenue in MOF catalysed water splitting lies in the exploitation of heterobinuclear charge transfer chromophores for visible light driven water oxidation. Frei *et al.* assembled $\text{TiOCr}^{\text{III}}$ metal-oxo clusters on the silica surface of MCM-41 to generate heterobinuclear metal-to-metal-charge-transfer chromophores with absorption in the visible range.⁹⁹ An IrO_2 doped derivative of the modified MCM-41 was observed to evolve dioxygen with a 13% η upon irradiation of an aqueous suspension of the catalyst. Photo-excitation of $\text{Ti}^{\text{IV}}\text{OCr}^{\text{III}}$ surface species into $\text{Ti}^{\text{III}}\text{OCr}^{\text{IV}}$ is believed to create acceptor sites poised to abstract electrons from the water oxidising IrO_2 nanoparticles. We recognise interesting parallels between the TiOCr clusters described by Frei and the titanium-oxo SBUs that are prevalent in MOFs such as MIL-125 (Ti), with molecular formula $\text{Ti}_8\text{O}_8(\text{OH})_4(\text{BDC})_6$ ($\text{BDC} = 1,4$ -benzenedicarboxylic acid). MOFs of this type possess rigid coordination environments conducive to establishing chromophoric sites by addition of metal dopants to SBUs or titanium-oxo functionalised organic linkers for example, and would also allow transport of reductive equivalents away from reactive sites courtesy of the framework's permeability.

MOF supported water reduction. MOFs offer convenient porous assemblies through which solution state electron donors and light sensitiser may be transmitted to encapsulated or tethered WRCs. Additionally, MOF linkers may be functionalised to be receptive to light of a specific wavelength, and certain MOF's are comprised of metal oxide SBUs that may directly mediate water reduction (see the preceding section). The MOF community have simulated water reduction aspects of the Z-scheme with considerable success, even going so far as to match WRCs with appropriate heterogeneous or homogeneous visible light sensitiser. In the following text we provide an account of recently developed photo-responsive MOFs that support catalytic water reduction. These may be broadly rationalised into four classes: MOFs containing tethered (heterogeneous) or untethered (homogeneous) organometallic catalysts, MOFs that carry out catalysis themselves via intrinsically active SBUs or linkers, and frameworks doped with dihydrogen evolving platinum nanoparticles. Much like its oxidation counter-part, catalysed water reduction requires facilitating agents such as electron acceptors, donors and light sensitiser.

In 2013 Cohen *et al.* reported photochemical dihydrogen production by UiO-66 decorated with the iron-only hydrogenase mimic $[\text{FeFe}](\text{dcbdt})(\text{CO})_6$ ($\text{dcbdt} = 1,4$ -dicarboxylbenzene-2,3-dithiolate).¹⁰⁰ Enterprisingly, the group used a mild post-synthetic exchange mechanism in degassed water to "swap out" 14% of the MOF's BDC linkers in favour of the dicarboxylic acid functionalised $[\text{FeFe}]$ hydrogenase mimic (see Fig. 5(a)). Catalytic activity of the new MOF, UiO-66- $[\text{FeFe}](\text{dcbdt})(\text{CO})_6$, plateaued at about 3.5 μmol of dihydrogen after one and a half hours when $[\text{Ru}(\text{bpy})_3]^{2+}$ was used as a light sensitiser and ascorbate as an electron donor in a pH 5 buffer solution. Despite catalytically limiting conditions, namely; recombination of excited states pertaining to $[\text{Ru}(\text{bpy})_2(\text{bpy})]^{+}$ and oxidised ascorbate, as well as impeded diffusion of the sensitiser; the activity of the MOF was still roughly three times better than that of the homogeneous adduct. Mechanistically, a two electron reduction of the $[\text{FeFe}]$ site seems improbable using a one-electron photosensitiser such as $[\text{Ru}(\text{bpy})_3]^{2+}$. Accordingly, the authors theorise disproportionation of singly reduced active sites (X^1), which go on to form catalytically active doubly reduced species (X^2). The MOF is credited with inhibiting recombination of charge equivalents by protecting the active sites. Given the restrictive pore size of UiO-66 (~ 8.5 Å),¹⁰¹ it seems unlikely that a surface-only species would derive protection from encapsulation, and more probable that a site isolation effect is responsible.

Feng *et al.* achieved similar conversions at 420 nm using a nicotinamide [FeFe] mimic ($[(\text{SCH}_2)_2\text{NC}(\text{O})\text{C}_5\text{H}_4\text{N}]-[\text{Fe}_2(\text{CO})_6]$) tethered to a zirconium porphyrin MOF (ZrPF) (ascorbic acid donor in pH 5 acetate buffer, Fig. 5(b)).¹⁰² The [FeFe]@ZrPF MOF was assembled by room temperature diffusion of the mimic into the MOF over 48 hours, after which time the distinctive fluorescence emission of the porphyrin moieties was quenched. The deactivation mechanism that occurs during catalysis remains unclear, although IR evidence indicates retention of CO bands and therefore possible preservation of the $\text{Fe}(\text{CO})_x$ groups. By comparison, the homogeneous adduct decomposes completely within 40 minutes under the same conditions.

Notably, both UiO-66 and ZrPF studies tether [FeFe] mimics via their bridgehead groups - a technique that does not enable participation of the bridging atom in catalysis. In 2013 Fontecave *et al.* established the catalytic significance of an aza-dithiolate bridgehead group in natural [FeFe] hydrogenase.^{103, 104} Armed with this discovery we anticipate that the MOF community will explore tethering of aza mimics via asymmetric ancillary sulphur or cyano ligands, thus generating more representative analogues of the natural system and improving on the existing catalytic models.

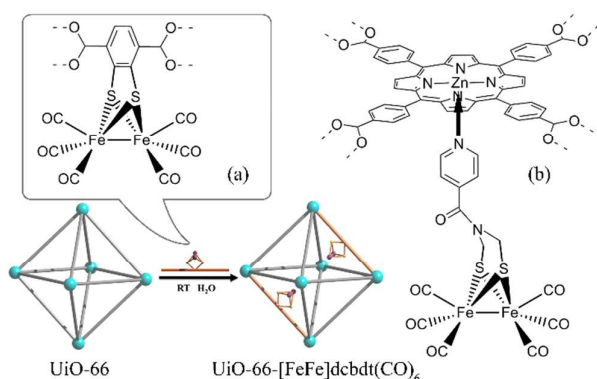


Fig. 5 Coordination modes of [FeFe] hydrogenase mimics (a) $[\text{FeFe}](\text{dcbdt})(\text{CO})_6$ (dcbdt = 1,4-dicarboxylbenzene-2,3-dithiolate) and (b) $[(\text{SCH}_2)_2\text{NC}(\text{O})\text{C}_5\text{H}_4\text{N}]-[\text{Fe}_2(\text{CO})_6]$ in UiO-66 and ZrPF type-MOFs, respectively. Adapted in part with permission from reference 56 © American Chemical Society.

Mori *et al.* contributed to the field with their $[\text{Ru}_2(p\text{-BDC})_2]_n$ and $[\text{Rh}_2(p\text{-BDC})_2]_n$ MOFs in 2009 and 2010 respectively.^{105, 106} The 2D ruthenium MOF is characterised by di-ruthenium paddlewheels interlinked by BDC. Tests for water reduction under visible light were positive using $[\text{Ru}(\text{bpy})_3]^{2+}$ as a sensitizer, MV^{2+} as an electron relay and Na_2EDTA to regenerate the photosensitizer. The MOF was 14.4 times more active than titania anatase, and roughly four times more active than the discrete paddlewheel $[\text{Ru}_2(\text{CH}_3\text{CO}_2)_4][\text{BF}_4]$, giving a final TON of 8.16 after four hours. A closely related rhodium analogue achieved comparable levels of dihydrogen production under the same conditions. The authors observe retardation of dihydrogen production when catalysis is carried out in the presence of competing coordinative anions such as acetate or chloride. On this basis they suggest that the axial positions of the paddlewheels are the sites responsible for catalysis.

$\text{Ru}(\text{bpy})_3]^{2+}$ light sensitizers may be incorporated directly into a MOF assembly and retain their classical absorptivities and one electron transfer photochemistry, as demonstrated by UiO-66 frameworks constructed from $\text{Ru}([2,2'\text{-bipyridine}]-5,5'\text{-dicarboxylic acid})_2\text{L}$ and $\text{Ru}([2,2'\text{-bipyridine}]-4,4'\text{-dicarboxylic acid})_2\text{L}$ linkers (where L = two cyanide groups or 2,2'-bipyridine).^{107, 108} Doping of light-sensitized MOFs with platinum nanoparticles has proven successful in the case of UiO-67 type materials prepared with “contracted” (H_2L_1 (2wt% loading)) and

“expanded” (H_2L_2 (100wt% loading)) linker groups of $[Ir(ppy)_2(bpy)]^+$ (ppy = 2-phenylpyridine, bpy = 2,2'-bipyridine-5,5'-dicarboxylate or 2,2'-bipyridine-5,5'-dibenzoate).¹⁰⁹ In their non-doped form the linkers of the resultant MOFs demonstrate visible light excitation up to a 1MLCT state with subsequent intersystem crossing to a 3MLCT state, followed by phosphorescent emission to the ground state. Lifetimes of the 3MLCT states for the contracted (MOF1) and expanded (MOF2) materials were 51.8 and 110.3 ns respectively, providing long-lived charge separation well disposed to injection of electrons into the conduction band of introduced platinum nanoparticles. UV-excitation of the iridium bipyridine linkers, proceeded by triethylamine quenching, formed $[Ir(ppy)(bpy^{\bullet-})]$ radicals capable of reducing K_2PtCl_4 directly inside the MOF pores. Relatively constricted MOF1 could accommodate three platinum atoms per linker relative to 240 for MOF2 (Fig. 6), although extensive framework distortion was observed for the latter due to the girth of the encapsulated platinum nanoparticles. A platinum to iridium ratio of approximately 18 was determined for the two doped $Pt@MOFs$. Under visible light irradiation, and in the presence of sacrificial reductant TEA, an $[Ir^{III}(ppy)_2(bpy^{\bullet-})]$ radical was generated from which electrons were subsequently transferred to platinum. $Pt@MOF2$ proved the more active catalytic system with a TON of 7000 after 48 hours. Both MOFs were more stable than their homogeneous analogues, suggesting that framework rigidity contributes significantly to stabilisation of sensitizer radical intermediates.

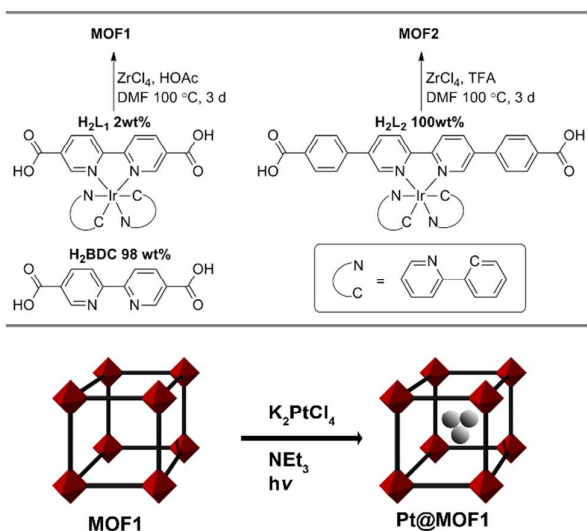


Fig. 6 Schematic for preparation of the light-sensitised UiO-67 materials “contracted” MOF1 (L_1 = 2wt%) and “expanded” MOF2 (L_2 = 100wt%), containing $Ir(ppy)(bpy)$ type linkers. Formation of $Pt@MOF1$ by impregnation of MOF1 with platinum nanoparticles.

Light sensitizers, such as the free base *meso*-tetra(4-carboxyl-phenyl) porphyrin (H_2TCPP) and its zinc metalated adduct ($ZnTCPP$), have been incorporated into MOFs as octadentate linkers tethered between $Al(OH)_4O$ chains.¹¹⁰ An irradiated suspension of MOF, colloidal platinum and sacrificial electron donor EDTA, induced reduction of the porphyrin rings and consequent relay of an electron to platinum (Fig. 7). Dihydrogen was subsequently generated at rates of $100 \mu\text{mol g}^{-1}\text{h}^{-1}$ ($ZnTCPP$) and $200 \mu\text{mol g}^{-1}\text{h}^{-1}$ (H_2TCPP). The low quantum yield of these systems was ascribed to self-quenching, which is evidently not prevented by the rigid segregation of porphyrin rings within the MOF structure. Mediation of an electron acceptor could theoretically delay charge recombination. However, mass transfer restrictions imposed by the tight $6 \times 11 \text{ \AA}^2$ MOF internal pore structure were shown to impede transport of methyl viologen (MV^{2+}) to platinum particles at the MOF surface.

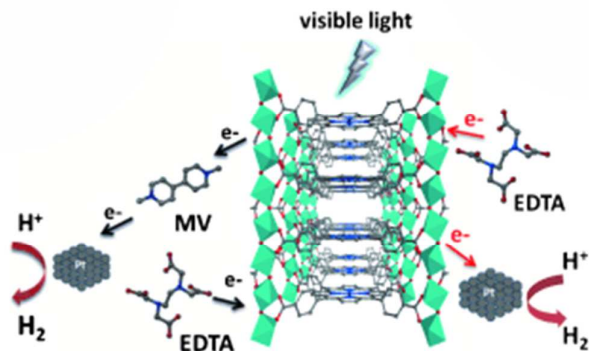


Fig. 7 Use of a light sensitive electron relay (H_2TCPP) tethered inside a MOF to promote dihydrogen evolution by colloidal platinum. Reproduced with permission from reference 66 © John Wiley and Sons.

MOF supported water reduction: delving into semiconducting systems. While most MOFs are insulating a small number do possess intrinsic semiconducting properties by virtue of the alignment between valence and conduction bands of their linker groups and SBUs, respectively (Fig. 8(a)). In order to carry out water splitting a photo-catalyst of this type requires a valence band with a potential more positive than that of the $\text{H}_2\text{O}/\text{O}_2$ couple (1.23 eV), and a conduction band less than that for the $\text{H}_2\text{O}/\text{H}_2$ couple (0.00 eV) (Fig. 8(b)).¹¹¹ As we will describe, the height of the VB may be manipulated by adjusting the chemical attributes of the linker, by employing BDC linkers with electron donating or withdrawing functional groups for example. Meanwhile, the energetic level of the conduction band is strongly influenced by the coordination geometry of metals making up the metal oxide SBUs, and there are even indications that coordinated solvents may influence this characteristic.¹¹² Two imperative requirements for a visible light sensitised semiconducting MOF are; photo-responsiveness of the linker within a 390-700 nm range, and efficient linker-to-cluster charge transfer without recombination of charges. In the case of water reducing MOFs, photo-excitation of linkers generates positive holes that are localised on the ligand (VB), and electrons that pass to the SBU (CB), where they are available to reduce H^+ . Water splitting by a visible light activated photo-catalyst in particular, requires a band gap smaller than 3.0 eV.⁹ Notably, titania possesses a band gap lower than this value and consequently has been studied extensively for its water splitting capabilities since the initial discovery by Honda and Fujishima.¹¹³ The titanium oxide SBUs in MIL-125 (Ti) have captured the imagination of the MOF community for this precise reason, fuelled by supporting computational studies. A recent DFT study by Walsh *et al.* interpolated the vertical ionisation potential for a series of MOFs using a normalised pore electrostatic potential.¹¹⁴ Tellingly, they observe a Type-II band offset for MOF-5 and MIL-125 relative to zinc oxide and titania, respectively, inferring improved hole and electron separation for these species.

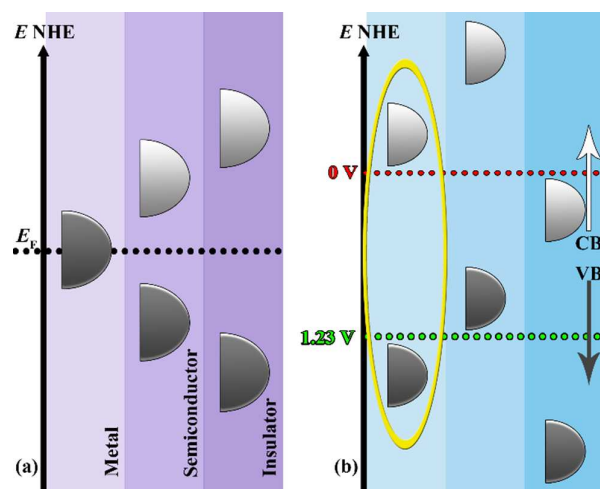
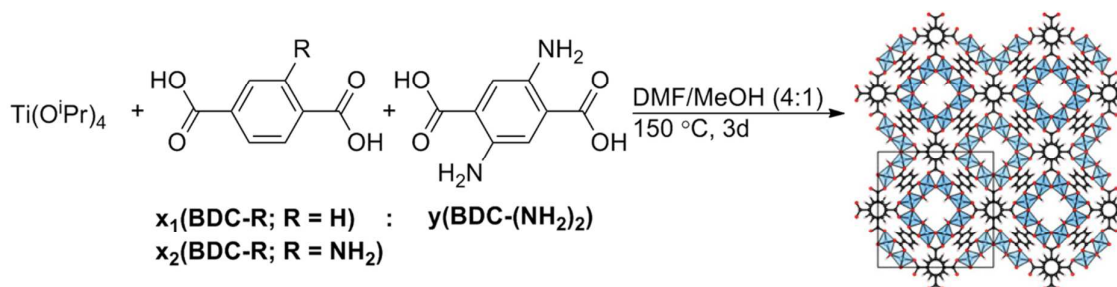


Fig. 8 (a) Schematic demonstrating conduction (CB) and valence (VB) band states for non-conducting, semiconducting and conducting materials with respect to Fermi level, and (b) band gap positions with respect to electrode potentials for water oxidation and reduction. The first panel presents an optimal band gap for water splitting, whereas the second and third panels describe respective scenarios where the valence band or conduction band are unsuitably positioned.

A combined synthetic and computational study published in 2013 emphasised the importance of linker functionalisation for controlling band gap in MIL-125 (Ti) (see Fig. 9).¹¹⁵ Materials prepared with 0, 10, 50 and 100% NH_2 -BDC and the differential quantity of BDC demonstrated a corollary increase in molar extinction coefficient. While the number of electron donating amine groups did little to change the band gap of the aminated bulk materials, calculations suggested that inclusion of one NH_2 -BDC linker per unit cell disrupted symmetry and induced splitting of the valence band (aromatic 2p orbitals) into multiple levels. The valence band of the 10% NH_2 -MIL-125 (Ti) adduct was consequently 1.2 eV higher than that for MIL-125 (Ti). By the same token a diaminated BDC linker $(\text{NH}_2)_2$ -BDC was more red-shifted than its mono-aminated analogue and increased the height of the valence band even further. A synthetically prepared 10% $(\text{NH}_2)_2$ -BDC 90% NH_2 -BDC MOF absorbed at 950 nm and possessed a valence band 2.45 eV higher than that of pure MIL-125 (Ti). Computational studies using a HSE06 hybrid functional indicated that band gaps may be decreased over a 1.1 eV range using 90% BDC mixed with 10% of alternatively substituted BDC-R linkers (where R: $-\text{CH}_3/-\text{Cl} > -\text{OH} > -\text{NH}_2 > \text{mixed amine} > -(\text{NH}_2)_2$).



Linker (%) $x_1 : x_2 : y$	100 : 0 : 0	90 : 10 : 0	80 : 20 : 0	50 : 50 : 0	0 : 100 : 0	0 : 90 : 10
Measured gap (eV)	3.68 (1)	2.75 (3)	2.55 (2)	2.62(1)	2.72(1)	1.23(2)

Fig. 9 Influence of BDC linker functionalisation upon the band gap of MIL-125 (Ti) type MOFs. Adapted with permission from reference 71 © American Chemical Society.

García *et al.* identified the latent semiconducting properties of the UiO-66 MOF and its bathochromically shifted amino adduct NH₂-UiO-66 when they used these materials to reduce methanol to dihydrogen under UV light.⁷³ Once platinum-doped these systems evolved almost triple the amount of dihydrogen compared to the parent assemblies. As a continuation of this work, Wang *et al.* tested a 1wt% platinum-doped UiO-66 MOF for H⁺ reduction under visible light, using the light sensitiser rhodamine B in the presence of triethanolamine.¹¹⁶ A maximum conversion of 116.0 μmol g⁻¹ h⁻¹ was obtained for a doped system which had undergone a washing step prior to catalysis. The authors propose a rational mechanism in which photo-excited rhodamine B injects electrons into the LUMO of the MOF, which then pass onto platinum nanoparticles where reduction of H⁺ is carried out. The low activity of the non-sensitised Pt@UiO-66 material suggests that direct transferral of electrons from the sensitiser to platinum accounts for much of the activity in the idealised system. The group went on to apply MIL-101 (Cr) as a solid support for semiconducting nanoparticles of cadmium sulfide and a platinum co-catalyst.¹¹⁷ TEM analysis revealed surface only deposition of the nanoparticles, and specifically, deposition of platinum on the cadmium sulfide particles rather than on the MOF surface. Under visible light in an electron donating lactic acid solution, a 10wt% cadmium sulfide embedded MOF doped with 0.5wt% platinum evolved approximately 150 μmol of dihydrogen per hour. The MOF itself demonstrated no semiconducting properties, but it did enhance the sensitisation of the chalcogenide by ensuring adequate dispersion of catalytic sites over its large surface area. By comparison, naked cadmium sulfide demonstrated about a fifth of the activity.

Inspired by Férey's account of UV photo-catalysed alcohol reduction by MIL-125 (Ti),¹¹⁸ Matsuoka *et al.* prepared bathochromically shifted NH₂-MIL-125 (Ti) and used the visible light sensitisation of the 2-amino benzenedicarboxylic acid in conjunction with a favourably aligned titanium oxide cluster conduction band to reduce H⁺.¹¹⁹ The linker to cluster charge transfer mechanism depends on triethanolamine as a sacrificial donor.¹²⁰ ESR spectra clearly indicated reversible reduction of the Ti⁴⁺ nuclei to Ti³⁺ in response to dihydrogen evolution and air oxidation. Even without dopant this system generated 5 μmol of dihydrogen at the titanium oxide cluster under visible light after three hours. Upon photo-deposition of platinum the amount of dihydrogen evolved doubled, indicating either a more favourable overlap of the platinum conduction band with the valence band of the linker, or improved charge separation as a result of inclusion of the platinum co-catalyst. Corollary experiments with platinum doped NH₂-UiO-66 (Zr) and MIL-125 (Ti) did not yield dihydrogen under visible light, suggesting that the combination of BDC-NH₂ linker and titanium oxide cluster is crucial to photo-catalytic dihydrogen evolution.

Coming full circle on the themes of this perspective, Gascon *et al.* recently reported a ship-in-the-bottle technique for assembly of dihydrogen evolving catalyst cobaloxime inside NH₂-MIL-125 (Ti).¹²¹ Consecutive migrations of the oxime ligand and CoBr₂·6H₂O into the MOF yielded Co@MOF with a 2.7wt% loading of Co, which equates to roughly one molecule of cobaloxime per cage. Under visible light Co@MOF delivered approximately 36 μmol of dihydrogen after 20 hours in a deoxygenated mixture of acetonitrile, triethylamine and water (5:1:0.1 v/v). The encapsulated catalyst was an order of magnitude more active than the MOF itself (Fig. 10(a)), whereas the molecular catalyst was completely inactive in the absence of a photosensitiser. Moreover, Co@MOF maintained a constant TOF of 0.8 h⁻¹ over 70 hours. The authors cannot yet offer conclusive evidence for an encapsulated homogeneous or heterogeneous active site, as poisoning experiments and photoluminescence spectroscopy present ambiguous results. Recycling indicated that the catalytic activity of the material is not attributed to homogeneous complex leached into the supernatant (Fig. 10(b)), although the 5-7 Å apertures of the MOF are arguably restrictive

enough to prevent such an event from occurring anyway. However, minor changes to the infrared amine stretching frequencies suggest that there are direct bonding interactions between the complex and the MOF.

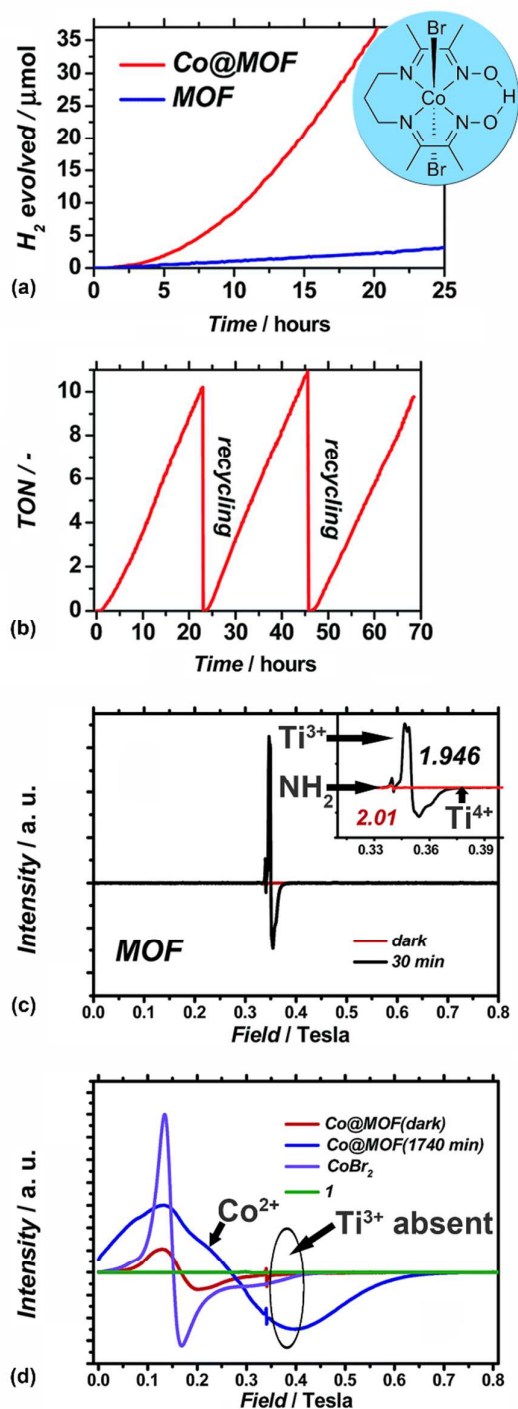


Fig. 10 (a) Dihydrogen detection by GC for Co@MOF and $\text{NH}_2\text{-MIL-125 (Ti)}$, (b) Catalytic recycling experiments with Co@MOF, (c) EPR spectra of $\text{NH}_2\text{-MIL-125 (Ti)}$, dark and photo-irradiated states, (d)

comparison of Co@MOF to reference species upon photo-irradiation (1 = cobaloxime complex). Adapted from reference 77 © with permission of The Royal Society of Chemistry.

EPR experiments were invaluable for differentiating Ti^{4+} (EPR silent) and Ti^{3+} ($g = 1.94$) transitions indicative of photo-excited transfer from the MOF linker to the SBU (Fig. 10(c)). Similarly, the irradiated Co@MOF evolved a high spin paramagnetic Co^{2+} signal from the EPR silent diamagnetic Co^{3+} initial species, which is consistent with the reported catalytic mechanism for homogeneous cobaloxime (Fig. 10(d)).¹²² Interestingly, the presence of the cobalt complex inside $\text{NH}_2\text{-MIL-125 (Ti)}$ completely suppressed the signal pertaining to titanium reduction, indicating efficient charge transfer from the titanium oxide clusters to the dihydrogen evolving cobalt complex.

Research involving MOF mediated water reduction is evidently advancing at a rapid rate. Photo-catalysed systems employing integrally sensitised MOF linkers or homogeneous photosensitisers have been reported. Moreover, evidence indicates that MOFs are not limited to a static scaffold-like role for supporting H^+ reducing noble metals, but may also tether or encapsulate molecular catalysts, or indeed catalyse reduction with the aid of internal metal oxide SBUs. We anticipate that a newly described NTU-9 (Ti) MOF will make a debut in water catalysed reduction before long, offering a narrow 1.74 eV band gap and alluring p-type semiconductor properties ideal for H^+ reduction into dihydrogen.¹²³

Conclusions

Our perspective summarises the most recent innovations in MOF supported water oxidation and reduction. A small group of MOFs are evidently robust and versatile players in the field of electrocatalytic, chemically promoted and photo-catalytic water splitting.

Electrocatalytic studies involving exotic new MOFs indicate that we can expect both catalysed water oxidation and reduction from innovatively configured frameworks containing relatively inexpensive metals. However, a thorough mechanistic investigation of these assemblies is still needed in order to illuminate the nature of their active sites. Without such information iterative improvements and adaptations are difficult.

MOFs have made a worthwhile contribution to the water oxidation debate. The rigid framework and defined internal dimensions of MIL-101 (Cr) in particular, are well-disposed toward encapsulation of highly active homogeneous water oxidation catalysts that suffer from intermolecular decomposition processes. In our view, the encapsulation approach could be a game-changer for chemically promoted homogeneous water oxidation, as it addresses the persistent stability problems that plague this field. Diffusion limitation remains a serious hurdle to transport of sensitisers and redox mediators where constricted frameworks are utilised. However, to the best of our knowledge no research groups have yet attempted to use MOF integrated light sensitisers in conjunction with catalysed water oxidation, a strategy that could very well resolve issues with premature charge recombination.

Water reduction supported by MOFs has ventured into stimulating new territory in recent years. UiO-67 (Zr) frameworks are capable of encapsulating platinum nanoparticles with a propensity for catalysing H^+ reduction. And the photo-responsive and conductive properties of some MOFs may be used to channel energy derived from visible light to catalytic sites. The $\text{NH}_2\text{-BDC}$ linker has distinguished itself as an adaptive moiety for light capture and band gap tuning in photo-catalytic MOFs. Moreover, Honda-Fujishima water splitting over titania has been assimilated into $\text{NH}_2\text{-MIL-125 (Ti)}$ type MOFs with some success, and further advancements may come from

development of efficient dopants, or adaptation of linker groups. We believe that there is still much mileage to be gained from the semiconductor attributes of MOFs, like MIL-125 (Ti), in photo-catalysed water reduction.

In spite of these significant findings, a fully integrated photo-catalysed MOF WOC and WRC capable of emulating nature's Z-scheme remains beyond our collective reach. Coupling of solar panels to an electrolytic cell may enable photo-electrocatalytic water oxidation and reduction mediated by MOFs. However, the complexity of an entirely photo-catalysed assembly – in which proximal donors and acceptors, and photo-generated holes and electrons cooperate without premature recombination – is self-evident and requires further innovation. The issue of gas separation in such a system similarly presents a serious challenge. Current research suggests that MOFs offer complimentary utility in water splitting processes. Their cavities seem well adapted for water oxidation whereas their frameworks seem better disposed toward water reduction. All things considered, MOFs have demonstrated a veritable “Swiss army knife” of attributes that lend them to the demanding water splitting process. With further fundamental research, particularly into the semiconducting properties of MOFs, it is our belief that these versatile materials will make a poignant contribution to the discourse on water splitting.

Acknowledgements

The support of a CCEM Hytech grant is gratefully acknowledged.

Notes and references

During the period between submission and revision of our manuscript a couple of examples of water reduction carried out by, or in the presence of MOFs, have appeared in the literature. We refer readers to the papers by: Du et al. concerning a nickel mercaptopyrimidine MOF with a TOF of 10.6 h⁻¹ in the presence of triethylamine and fluorescein under blue light,¹²⁴ and Chen et al. describing a photosensitised MOF encapsulating a platinum dihydrogen evolving catalyst (Ru–Pt@UiO-67).¹²⁵ ^aDepartment of Chemistry and Applied Biosciences, Institute for Chemical and Bioengineering, ETH Zürich, Wolfgang-Pauli-Str. 10, CH-8093 Zürich, Switzerland; ^bPaul Scherrer Institute, Villigen, CH-5232, Switzerland. E-mail: jeroen.vanbokhoven@chem.ethz.ch; Tel: +41 (0)44 632 5542. E-mail: marco.ranocchiaro@psi.ch; Tel: +41 (0)56 310 58 43.

1. M. E. Mann, Z. Zhang, M. K. Hughes, R. S. Bradley, S. K. Miller, S. Rutherford and F. Ni, *PNAS*, 2008, 105, 13252-13257.
2. C. M. Kalamaras and A. M. Efstathiou, *Conference Papers in Energy*, 2013, 2013, 9.
3. B. C. R. Ewan and R. W. K. Allen, *Int. J. Hydrogen Energy*, 2005, 30, 809-819.
4. J. Turner, G. Sverdrup, M. K. Mann, P.-C. Maness, B. Kroposki, M. Ghirardi, R. J. Evans and D. Blake, *Int. J. Energy Res.*, 2008, 32, 379-407.
5. P. Du and R. Eisenberg, *Energy Environ. Sci.*, 2012, 5, 6012-6021.
6. M. D. Kärkäs, O. Verho, E. V. Johnston and B. Åkermark, *Chem. Rev.*, 2014, 114, 11863-12001.
7. A. Llobet, ed., *Molecular Water Oxidation Catalysis: A key topic for new sustainable energy conversion schemes*, John Wiley & Sons, Ltd., West Sussex, United Kingdom, 2014.
8. S. Losse, J. G. Vos and S. Rau, *Coord. Chem. Rev.*, 2010, 254, 2492-2504.
9. A. Kudo and Y. Miseki, *Chem. Soc. Rev.*, 2009, 38, 253-278.
10. W. A. Hermann, *Energy*, 2006, 31, 1685-1702.
11. S. T. Stripp and T. Happe, *Dalton Trans.*, 2009, 9960-9969.
12. G. C. Dismukes, R. Brimblecombe, G. A. N. Felton, R. S. Pryadun, J. E. Sheats, L. Spiccia and G. F. Swiegers, *Acc. Chem. Res.*, 2009, 42, 1935-1943.
13. G. Renger, *Biochimica et Biophysica Acta (BBA) - Bioenergetics*, 2012, 1817, 1164-1176.
14. J. Barber and B. Andersson, *Nature*, 1994, 370, 31-34.
15. Y. Tachibana, L. Vayssieres and J. R. Durrant, *Nat Photon*, 2012, 6, 511-518.
16. K. J. Young, L. A. Martini, R. L. Milot, R. C. Snoeberger Iii, V. S. Batista, C. A. Schmuttenmaer, R. H. Crabtree and G. W. Brudvig, *Coord. Chem. Rev.*, 2012, 256, 2503-2520.
17. S. Hu, C. Xiang, S. Haussener, A. D. Berger and N. S. Lewis, *Energy Environ. Sci.*, 2013, 6, 2984-2993.
18. M. G. Walter, E. L. Warren, J. R. McKone, S. W. Boettcher, Q. Mi, E. A. Santori and N. S. Lewis, *Chem. Rev.*, 2010, 110, 6446-6473.
19. X. Yang, R. Liu, Y. He, J. Thorne, Z. Zheng and D. Wang, *Nano Res.*, 2015, 8, 56-81.
20. J. Luo, J.-H. Im, M. T. Mayer, M. Schreier, M. K. Nazeeruddin, N.-G. Park, S. D. Tilley, H. J. Fan and M. Grätzel, *Science*, 2014, 345, 1593-1596.
21. S. N. Habisreutinger, T. Leijtens, G. E. Eperon, S. D. Stranks, R. J. Nicholas and H. J. Snaith, *Nano Letters*, 2014, 14, 5561-5568.

22. J. Brilliet, J.-H. Yum, M. Cornuz, T. Hisatomi, R. Solaraska, J. Augustynski, M. Graetzel and K. Sivula, *Nat Photon*, 2012, 6, 824-828.
23. J.-H. Yum, E. Baranoff, F. Kessler, T. Moehl, S. Ahmad, T. Bessho, A. Marchioro, E. Ghadiri, J.-E. Moser, C. Yi, M. K. Nazeeruddin and M. Grätzel, *Nature Commun.*, 2012, 3, 631.
24. O. Khaselev and J. A. Turner, *Science*, 1998, 280, 425-427.
25. S. Y. Reece, J. A. Hamel, K. Sung, T. D. Jarvi, A. J. Esswein, J. J. H. Pijpers and D. G. Nocera, *Science*, 2011, 334, 645-648.
26. D. G. Nocera, *Acc. Chem. Res.*, 2012, 45, 767-776.
27. C. R. Cox, J. Z. Lee, D. G. Nocera and T. Buonassisi, *PNAS*, 2014, 111, 14057-14061.
28. S. Hu, M. R. Shaner, J. A. Beardslee, M. Lichterman, B. S. Brunschwig and N. S. Lewis, *Science*, 2014, 344, 1005-1009.
29. R. E. Rocheleau, E. L. Miller and A. Misra, *Energy & Fuels*, 1998, 12, 3-10.
30. C. Liu, J. Tang, H. M. Chen, B. Liu and P. Yang, *Nano Letters*, 2013, 13, 2989-2992.
31. M. R. Shaner, K. T. Fountaine, S. Ardo, R. H. Coridan, H. A. Atwater and N. S. Lewis, *Energy Environ. Sci.*, 2014, 7, 779-790.
32. J. Y. Kim, G. Magesh, D. H. Youn, J.-W. Jang, J. Kubota, K. Domen and J. S. Lee, *Sci. Rep.*, 2013, 3.
33. F. F. Abdi, L. Han, A. H. M. Smets, M. Zeman, B. Dam and R. van de Krol, *Nature Commun.*, 2013, 4.
34. O. M. Yaghi, G. Li and H. Li, *Nature*, 1995, 378, 703-706.
35. H. W. Langmi, J. Ren, B. North, M. Mathe and D. Bessarabov, *Electrochimica Acta*, 2014, 128, 368-392.
36. A. Schneemann, V. Bon, I. Schwedler, I. Senkovska, S. Kaskel and R. A. Fischer, *Chem. Soc. Rev.*, 2014, 43, 6062-6096.
37. E. Coronado and G. Minguez Espallargas, *Chem. Soc. Rev.*, 2013, 42, 1525-1539.
38. G. Givaja, P. Amo-Ochoa, C. J. Gomez-Garcia and F. Zamora, *Chem. Soc. Rev.*, 2012, 41, 115-147.
39. Y. Cui, Y. Yue, G. Qian and B. Chen, *Chem. Rev.*, 2012, 112, 1126-1162.
40. M. Fuentes-Cabrera, D. M. Nicholson, B. G. Sumpter and M. Widom, *The Journal of Chemical Physics*, 2005, 123, 124713.
41. B. Civalieri, F. Napoli, Y. Noel, C. Roetti and R. Dovesi, *CrystEngComm*, 2006, 8, 364-371.
42. S. Furukawa, J. Reboul, S. Diring, K. Sumida and S. Kitagawa, *Chem. Soc. Rev.*, 2014, 43, 5700-5734.
43. F. L. Morel, X. Xu, M. Ranocchiaro and J. A. v. Bokhoven, in *Chemistry of organo-hybrids: Synthesis and characterization of functional nano-objects*, ed. C. C. B. Charleux, E. Lacôte, John Wiley & Sons, Hoboken, New Jersey, 2015, ch. 6, pp. 200-232.
44. C. E. Wilmer, M. Leaf, C. Y. Lee, O. K. Farha, B. G. Hauser, J. T. Hupp and R. Q. Snurr, *Nat. Chem.*, 2012, 4, 83-89.
45. V. Stavila, A. A. Talin and M. D. Allendorf, *Chem. Soc. Rev.*, 2014, 43, 5994-6010.
46. C. H. Hendon, D. Tiana and A. Walsh, *PCCP*, 2012, 14, 13120-13132.
47. M. T. M. Koper, *J. Electroanal. Chem.*, 2011, 660, 254-260.
48. M. Ranocchiaro and J. A. v. Bokhoven, *PCCP*, 2011, 13, 6388-6396.
49. J. Gascon, A. Corma, F. Kapteijn and F. X. Llabrés i Xamena, *ACS Catal.*, 2013, 4, 361-378.
50. T. Zhang and W. Lin, *Chem. Soc. Rev.*, 2014, 43, 5982-5993.
51. C. G. Silva, A. Corma and H. Garcia, *J. Mater. Chem.*, 2010, 20, 3141-3156.
52. N. Dubey, N. K. Labhsetwar, S. Devotta and S. S. Rayalu, *Catal. Today*, 2007, 129, 428-434.
53. M. Álvaro, J. F. Cabeza, D. Fabuel, H. García, E. Guíjarro and J. L. Martínez de Juan, *Chem. Mater.*, 2006, 18, 26-33.
54. A. Corma and H. Garcia, *Chem. Commun.*, 2004, 13, 1443-1459.
55. P. Koning, in *Pioneering path to electrical conductivity in 'Tinkertoy' materials to appear in Science*, Sandia National Laboratories, California, Livermore, 2013.
56. J. B. DeCoste, G. W. Peterson, H. Jasuja, T. G. Glover, Y.-g. Huang and K. S. Walton, *J. Mater. Chem. A*, 2013, 1, 5642-5650.
57. J. Canivet, A. Fateeva, Y. Guo, B. Coasne and D. Farrusseng, *Chem. Soc. Rev.*, 2014, 43, 5594-5617.
58. N. C. Burtch, H. Jasuja and K. S. Walton, *Chem. Rev.*, 2014, 114, 10575-10612.
59. F. B. Baker, T. W. Newton and M. Kahn, *J. Phys. Chem.*, 1960, 64, 109-112.
60. C. E. Wilmer, M. Leaf, C. Y. Lee, O. K. Farha, B. G. Hauser, J. T. Hupp and R. Q. Snurr, *Nat. Chem.*, 2012, 4, 83-89.
61. L. Valenzano, B. Civalieri, S. Chavan, S. Bordiga, M. H. Nilsen, S. Jakobsen, K. P. Lillerud and C. Lamberti, *Chem. Mater.*, 2011, 23, 1700-1718.
62. J. H. Cavka, S. Jakobsen, U. Olsbye, N. Guillou, C. Lamberti, S. Bordiga and K. P. Lillerud, *JACS*, 2008, 130, 13850-13851.
63. Q. Liu, L. Ning, S. Zheng, M. Tao, Y. Shi and Y. He, *Sci. Rep.*, 2013, 3.
64. G. Férey, C. Mellot-Draznieks, C. Serre, F. Millange, J. Dutour, S. Surlblé and I. Margiolaki, *Science*, 2005, 309, 2040-2042.
65. P. Serra-Crespo, E. V. Ramos-Fernandez, J. Gascon and F. Kapteijn, *Chem. Mater.*, 2011, 23, 2565-2572.
66. J. Gascon, U. Aktay, M. D. Hernandez-Alonso, G. P. M. van Klink and F. Kapteijn, *J. Catal.*, 2009, 261, 75-87.
67. C. Serre, F. Millange, C. Thouvenot, M. Nogués, G. Marsolier, D. Louër and G. Férey, *JACS*, 2002, 124, 13519-13526.
68. Y. Fu, D. Sun, Y. Chen, R. Huang, Z. Ding, X. Fu and Z. Li, *Angew. Chem. Int. Ed.*, 2012, 51, 3364-3367.
69. K. S. Park, Z. Ni, A. P. Côté, J. Y. Choi, R. Huang, F. J. Uribe-Romo, H. K. Chae, M. O'Keeffe and O. M. Yaghi, *PNAS*, 2006, 103, 10186-10191.

70. D. Feng, Z.-Y. Gu, J.-R. Li, H.-L. Jiang, Z. Wei and H.-C. Zhou, *Angew. Chem. Int. Ed.*, 2012, 51, 10307-10310.
71. M. Bosch, M. Zhang and H.-C. Zhou, *Adv. Chem.*, 2014, 2014, 8.
72. A. Marti, M. Van and K. Balkus, Jr., *J. Porous Mater.*, 2014, 21, 889-902.
73. C. Gomes Silva, I. Luz, F. X. Llabrés i Xamena, A. Corma and H. García, *Chem. Eur. J.*, 2010, 16, 11133-11138.
74. K. S. Joya, Y. F. Joya, K. Ocakoglu and R. van de Krol, *Angew. Chem. Int. Ed.*, 2013, 52, 10426-10437.
75. R. L. Doyle, I. J. Godwin, M. P. Brandon and M. E. G. Lyons, *PCCP*, 2013, 15, 13737-13783.
76. T. W. Woolerton, S. Sheard, Y. S. Chaudhary and F. A. Armstrong, *Energy Environ. Sci.*, 2012, 5, 7470-7490.
77. A. Braun, F. Boudoire, D. K. Bora, G. Faccio, Y. Hu, A. Kroll, B. S. Mun and S. T. Wilson, *Chem. Eur. J.*, 2014, 20, 1-13.
78. Y. Gong, T. Wu, P. G. Jiang, J. H. Lin and Y. X. Yang, *Inorg. Chem.*, 2012, 52, 777-784.
79. X.-L. Hu, C.-Y. Sun, C. Qin, X.-L. Wang, H.-N. Wang, E.-L. Zhou, W.-E. Li and Z.-M. Su, *Chem. Commun.*, 2013, 49, 3564-3566.
80. Y. Gong, Z. Hao, J. Meng, H. Shi, P. Jiang, M. Zhang and J. Lin, *ChemPlusChem*, 2014, 79, 266-277.
81. Y. Gong, H.-F. Shi, P.-G. Jiang, W. Hua and J.-H. Lin, *Cryst. Growth Des.*, 2013, 14, 649-657.
82. S. Wang, Y. Hou, S. Lin and X. Wang, *Nanoscale*, 2014, 6, 9930-9934.
83. E. Sellì, G. L. Chiarello, E. Quartarone, P. Mustarelli, I. Rossetta and L. Fornia, *Chem. Commun.*, 2007, 47, 5022-5024.
84. D. Jiang, H. Zhao, S. Zhang and R. John, *J. Phys. Chem. B*, 2003, 107, 12774-12780.
85. P. Falcaro, R. Ricco, C. M. Doherty, K. Liang, A. J. Hill and M. J. Styles, *Chem. Soc. Rev.*, 2014, 43, 5513-5560.
86. M. D. Symes and L. Cronin, *Nat. Chem.*, 2013, 5, 403-409.
87. H. Zhang, S. Chobot, A. Osyczka, C. A. Wraight, P. L. Dutton and C. Moser, *Journal of bioenergetics and biomembranes*, 2008, 40, 493-499.
88. B. Rausch, M. D. Symes and L. Cronin, *JACS*, 2013, 135, 13656-13659.
89. B. Rausch, M. D. Symes, G. Chisholm and L. Cronin, *Science*, 2014, 345, 1326-1330.
90. J. Limburg, J. S. Vrettos, H. Chen, J. C. de Paula, R. H. Crabtree and G. W. Brudvig, *JACS*, 2000, 123, 423-430.
91. R. E. Hansen and S. Das, *Energy Environ. Sci.*, 2014, 7, 317-322.
92. B. Nepal and S. Das, *Angew. Chem. Int. Ed.*, 2013, 52, 7224-7227.
93. C. Wang, J.-L. Wang and W. Lin, *JACS*, 2012, 134, 19895-19908.
94. C. Wang, Z. Xie, K. E. deKrafft and W. Lin, *JACS*, 2011, 133, 13445-13454.
95. D. J. Xiao, E. D. Bloch, J. A. Mason, W. L. Queen, M. R. Hudson, N. Planas, J. Borycz, A. L. Dzubak, P. Verma, K. Lee, F. Bonino, V. Crocellà, J. Yano, S. Bordiga, D. G. Truhlar, L. Gagliardi, C. M. Brown and J. R. Long, *Nat. Chem.*, 2014, 6, 590-595.
96. W. C. Ellis, N. D. McDaniel, S. Bernhard and T. J. Collins, *JACS*, 2010, 132, 10990-10991.
97. L. Duan, F. Bozoglian, S. Mandal, B. Stewart, T. Privalov, A. Llobet and L. Sun, *Nat. Chem.*, 2012, 4, 418-423.
98. B. Li, F. Li, S. Bai, Z. Wang, L. Sun, Q. Yang and C. Li, *Energy Environ. Sci.*, 2012, 5, 8229-8233.
99. H. Frei, *CHIMIA International Journal for Chemistry*, 2009, 63, 721-730.
100. S. Pullen, H. Fei, A. Orthaber, S. M. Cohen and S. Ott, *JACS*, 2013, 135, 16997-17003.
101. M. J. Katz, Z. J. Brown, Y. J. Colon, P. W. Siu, K. A. Scheidt, R. Q. Snurr, J. T. Hupp and O. K. Farha, *Chem. Commun.*, 2013, 49, 9449-9451.
102. K. Sasan, Q. Lin, C. Mao and P. Feng, *Chem. Commun.*, 2014, 50, 10390-10393.
103. D. Schilter and T. B. Rauchfuss, *Angew. Chem. Int. Ed.*, 2013, 52, 13518-13520.
104. G. Berggren, A. Adamska, C. Lambert, T. R. Simmons, J. Esselborn, M. Atta, S. Gambarelli, J. M. Mouesca, E. Reijerse, W. Lubitz, T. Happe, V. Artero and M. Fontecave, *Nature*, 2013, 499, 66-69.
105. Y. Kataoka, K. Sato, Y. Miyazaki, K. Masuda, H. Tanaka, S. Naito and W. Mori, *Energy Environ. Sci.*, 2009, 2, 397-400.
106. W. Mori, Y. Kataoka, K. Sato, Y. Miyazaki, Y. Suzuki, H. Tanaka, Y. Kitagawa, T. Kawakami and M. Okumura, *Chem. Lett.*, 2010, 39, 358-359.
107. C. A. Kent, D. Liu, L. Ma, J. M. Papanikolas, T. J. Meyer and W. Lin, *JACS*, 2011, 133, 12940-12943.
108. C. A. Kent, D. Liu, T. J. Meyer and W. Lin, *JACS*, 2012, 134, 3991-3994.
109. C. Wang, K. E. deKrafft and W. Lin, *JACS*, 2012, 134, 7211-7214.
110. A. Fateeva, P. A. Chater, C. P. Ireland, A. A. Tahir, Y. Z. Khimiyak, P. V. Wiper, J. R. Darwent and M. J. Rosseinsky, *Angew. Chem. Int. Ed.*, 2012, 51, 7440-7444.
111. Y. Wu, M. Chan and G. Ceder, *Phys. Rev. B: Condens. Matter*, 2011, 83, 235301.
112. K. S. Asha, P. R. Kavyasree, A. George and S. Mandal, *Dalton Trans.*, 2015, 44, 1009-1016.
113. A. Fujishima and K. Honda, *Nature*, 1972, 238, 37.
114. K. T. Butler, C. H. Hendon and A. Walsh, *JACS*, 2014, 136, 2703-2706.
115. C. H. Hendon, D. Tiana, M. Fontecave, C. Sanchez, L. D'arras, C. Sassoie, L. Rozes, C. Mellot-Draznieks and A. Walsh, *JACS*, 2013, 135, 10942-10945.
116. J. He, J. Wang, Y. Chen, J. Zhang, D. Duan, Y. Wang and Z. Yan, *Chem. Commun.*, 2014, 50, 7063-7066.
117. J. He, Z. Yan, J. Wang, J. Xie, L. Jiang, Y. Shi, F. Yuan, F. Yu and Y. Sun, *Chem. Commun.*, 2013, 49, 6761-6763.
118. M. Dan-Hardi, C. Serre, T. Frot, L. Rozes, G. Maurin, C. Sanchez and G. Férey, *JACS*, 2009, 131, 10857-10859.
119. Y. Horiuchi, T. Toyao, M. Saito, K. Mochizuki, M. Iwata, H. Higashimura, M. Anpo and M. Matsuoka, *J. Phys. Chem. C*, 2012, 116, 20848-20853.
120. M. de Miguel, F. Ragon, T. Devic, C. Serre, P. Horcajada and H. García, *ChemPhysChem*, 2012, 13, 3651-3654.
121. M. A. Nasalevich, R. Becker, E. V. Ramos-Fernandez, S. Castellanos, S. L. Veber, M. V. Fedin, F. Kapteijn, J. N. H. Reek, J. I. van der Vlugt and J. Gascon, *Energy Environ. Sci.*, 2015, 8, 364-375.

122. J. L. Dempsey, B. S. Brunshwig, J. R. Winkler and H. B. Gray, *Acc. Chem. Res.*, 2009, 42, 1995-2004.
123. J. Gao, J. Miao, P.-Z. Li, W. Y. Teng, L. Yang, Y. Zhao, B. Liu and Q. Zhang, *Chem. Commun.*, 2014, 50, 3786-3788.
124. Y. Feng, C. Chen, Z. Liu, B. Fei, P. Lin, Q. Li, S. Sun and S. Du, *J. Mater. Chem. A*, 2015, 3, 7163-7169.
125. C.-C. Hou, T.-T. Li, S. Cao, Y. Chen and W.-F. Fu, *J. Mater. Chem. A*, 2015, 19, 10386-10394.

